Hydrol. Earth Syst. Sci. Discuss., 12, 2975–3010, 2015
www.hydrol-earth-syst-sci-discuss.net/12/2975/2015/
doi:10.5194/hessd-12-2975-2015

Hydrology and Earth System Sciences
Discussions
Open Access

On the spatial organization of the ridge slough patterned landscape

S. T. Casey[1], M. J. Cohen[1], S. Acharya[1], D. A. Kaplan[2], and J. W. Jawitz[3]

[1]School of Forest Resources and Conservation, University of Florida, Gainesville FL, USA
[2]Environmental Engineering Sciences, University of Florida, Gainesville FL, USA
[3]Soil and Water Science Department, University of Florida, Gainesville, FL, USA

Received: 19 February 2015 – Accepted: 24 February 2015 – Published: 16 March 2015

Correspondence to: M. J. Cohen (mjc@ufl.edu)

Published by Copernicus Publications on behalf of the European Geosciences Union.

Abstract

A century of hydrologic modification has altered the physical and biological drivers of landscape processes in the Everglades (southern Florida, USA). Restoring the ridge-slough patterned landscape, a dominant feature of the historical system, is a priority, but requires an understanding of pattern genesis mechanisms. Physical experiments to evaluate alternative pattern formation mechanisms are limited by the time scales of peat accumulation and loss, necessitating model-based comparisons, where support for a particular mechanism is based on model replication of extant patterning and trajectories of degradation. However, multiple mechanisms yield a central feature of ridge-slough patterning (patch elongation in the direction of historical flow), limiting the utility of that characteristic for discriminating among alternatives. Using data from vegetation maps we investigated the statistical features of ridge-slough spatial patterning (ridge density, patch perimeter, elongation, patch-area scaling, and spatial periodicity) to establish rigorous criteria for evaluating model performance, and to inform controls on pattern variation across the contemporary system. Mean water depth explained significant variation in ridge density, total perimeter, and length : width ratios, illustrating significant pattern response to existing hydrologic gradients. Two independent analyses (2-D periodograms and patch size distributions) provide strong evidence against regular patterning, with the landscape exhibiting neither a characteristic wavelength nor a characteristic patch size, both of which are expected under conditions that produce regular patterns. Rather, landscape properties suggest robust scale-free patterning, indicating genesis from the coupled effects of local facilitation and a global negative feedback operating uniformly at the landscape-scale. Critically, this challenges widespread invocation of meso-scale negative feedbacks for explaining ridge-slough pattern origins. These results help discern among genesis mechanisms and provide an improved statistical template against which to compare model outputs, as well as landscape trajectories with future restoration.

1 Introduction

The coupling of ecosystem processes operating at different scales can cause vegetation communities to form a wide variety of spatial patterns (Borgogno et al., 2009; Eppinga et al., 2010), ranging from highly regular striping, stippling or maze-like patterns in woodland landscapes (Ludwig et al., 1999), tidal mud flats (Weerman et al., 2012), and boreal peatlands (Eppinga et al., 2009) to scale-free patterning in semi-arid landscapes (Kefi et al., 2007; Scanlon et al., 2007). The mechanisms that produce these patterns are integral to understanding landscape origins, and thus for predicting appropriate remedies where patterns have been degraded and require restoration. The spatial arrangement of vegetation on the landscape has long been viewed as a manifestation of the dominant interactions and drivers (Hutchinson, 1957; Levin, 1992), and the scales at which they operate. By quantifying this spatial arrangement we can make process-based inferences about the underlying mechanisms (Gardner et al., 1987; Turner, 2005).

The ridge-slough landscape composed ∼ 55 % of the pre-development Everglades at the tip of the Florida peninsula (McVoy et al., 2011). However, the processes that created, and in some places still maintain, the characteristic ridge-slough patterning are only partially understood (Science Coordination Team, 2003; Larsen et al., 2011; Cohen et al., 2011). The landscape pattern consists of flow-parallel bands of higher-elevation ridges dominated by the emergent sedge sawgrass (*Cladium jamaicense*), interspersed within a matrix of lower-elevation (ca. 25 cm lower in the best conserved portions of the landscape; Watts et al., 2010) sloughs containing a variety of submerged and emergent herbaceous macrophytes. The Everglades has undergone massive hydrologic modification through the construction of a system of levees and canals (Light and Dineen, 1994) and the ensuing ecological degradation has prompted a complex, expensive, and ambitious restoration effort. Because the ridge-slough landscape was so prevalent in the pre-development system, pattern restoration is a central priority (SCT 2003; McVoy et al., 2011). The mechanisms that control the emergence of patterning, and explain variation in pattern geometry are thus integral to specifying hydrologic restoration objectives.

To understand the landscape processes that produce patterning, and by extension gain insight into how to restore them (Pickett and Cadenasso, 1995), requires a testable mechanistic framework for pattern genesis and maintenance. However, experiments to test alternative mechanisms are constrained by the spatial extent and time scales of peat accumulation responses. Paradoxically, compartmentalization by the extensive canal and levee system has created artificial gradients that are informative for assessing trajectories of landscape pattern degradation. Here we focus on Water Conservation Area 3 (WCA-3), located in the central Everglades, an area historically dominated by the ridge-slough landscape (Fig. 1), and where the best conserved patterning is found. The hydrologic gradient in WCA-3 spans from relatively dry (i.e., short hydroperiod) conditions in the north due to major canals that drain water to the southeast, and excessive inundation (i.e., long hydroperiod) in the south and southeast due to impoundment caused by US41/Tamiami Trail (which runs orthogonal to flow) and the L-67 levee. The best conserved patterning (SCT, 2003) is found between these two hydrologic extremes.

Several alternative hypotheses have been proposed to explain ridge slough patterns; all have been evaluated using process-based models. The mechanisms invoked vary between alternatives, and include evaporative nutrient redistribution (Ross et al., 2006), flow-driven sediment redistribution from sloughs to ridges (Larsen, 2007; Lago et al., 2010), ponding induced long-range inhibition (Cheng et al., 2011), self-optimization of patterning for discharge and hydroperiod (Cohen et al., 2011; Kaplan et al., 2012; Heffernan et al., 2013), and a suite of mechanisms that couple pattern-hydroperiod effects with anisotropic local contagion processes (Acharya et al., 2015). Clearly, these mechanisms are not mutually exclusive, so process models have sought to explore the sufficiency of each alternative, while acknowledging the potential that multiple processes may overlap. One central criterion used to evaluate the models has been whether simulations can produce morphologies qualitatively consistent with the extant landscape (principally replicating the elongation of patches in the flow direction). To date, however, almost all models either accomplish (Ross et al., 2006; Larsen and Harvey, 2010; Lago et al., 2010; Cheng et al., 2011; Acharya et al., 2015) or strongly imply (Heffernan et al., 2013) this, limiting the ability to discriminate between pattern genesis mechanisms and highlighting the need for a more rigorous and quantitative characterization of landscape pattern.

To better characterize the extant pattern (both the best conserved state and along varying trajectories of degradation) requires spatial analyses that yield quantitative properties against which model outputs can be compared. Although numerous metrics have been developed to quantify different pattern attributes (Wu et al., 2007; Yuan et al., 2015), significant gaps in our understanding of how to interpret these metrics remain (Turner, 2001; Remmel and Csillag, 2003). Real landscapes clearly depart from regular Euclidean geometry, making characterization problematic in some cases (Mandelbrot, 1983). Likewise, changes in mapping procedures (e.g., grain size, extent, classification schemes) can yield significantly different metric values for the same landscape (Li and Wu, 2004). To remedy some of these issues, we focused on a set of relatively direct and easily interpreted metrics of fundamental aspects of the pattern, and used multiple maps produced with varying methods to rule out mapping-related artifacts.

We were interested in three aspects of landscape patterning: prevalence statistics, patch scaling relationships, and spectral (i.e., pattern wavelength) characteristics. For each aspect, we explored the magnitude of site-to-site variation and hydrologic controls on that variation.

Prevalence statistics focus on what is likely the most basic and intuitive geometric properties of the landscape: areal coverage of the patch types, landscape pattern complexity (perimeter), and the degree of elongation. While inundation has been shown to control species composition (Givnish et al., 2008; Zweig and Kitchens, 2008; Todd et al., 2010), the relationship of hydrologic drivers to other aspects of landscape pattern remain relatively unknown, so this effort also serves as an inventory of hydrologic controls on pattern geometry.

Patch scaling relationships examine properties of individual ridge patches (where patches are defined as groups of contiguous occupied cells) and how they vary with patch area. They are of particular interest because patch–scaling relationships can yield information about the scale and strength of spatial mechanisms at work (Mandelbrot, 1983; Nikora, 1998). For example, length measurements (e.g., perimeter) that scale to area according to a power-function (i.e., $y = x^{\alpha}$, where α is a scaling parameter) or geometric measurements that remain invariant with patch size (such as relative elongation) are found in fractals (Lovejoy, 1982), suggesting genesis mechanisms that operate equally at all scales. Conversely, the absence of power-law scaling may indicate that dominant genesis mechanisms operate at a specific, definable, scale.

Patch size distributions (i.e., relative prevalence of different patch sizes) have been used in many systems to inform underlying landscape processes (e.g., Manor and Shnerb, 2008a; Kefi et al., 2011; Bowker and Maestre, 2012; Weerman et al., 2012). For example, regular patterning is associated with a characteristic patch size (Rietkerk and van de Koppel, 2008; von Hardenberg, 2010), arising in response to an inhibitory feedback operating at a particular spatial scale (van de Koppel and Crain, 2002) that limits patch expansion. Under these conditions, there should be a distinct mode in patch area distribution, or at least the absence of very large patches (Manor and Shnerb, 2008; von Hardenberg, 2010; Kefi et al., 2014). In contrast, patch size distributions that follow a power-law show no characteristic spatial scale (e.g., Scanlon et al., 2007); that is, they are scale-free, in that the distribution form remains the same regardless of the measurement scale.

Scale-free distributions can arise via a number of mechanisms (Newman et al., 2005). In a landscape where grid cells are randomly occupied, patch distributions show relatively few large patches, up to a critical density (~ 0.59; known as the percolation threshold) at which patches span the domain, yielding power-law area scaling. At densities slightly above and below the percolation threshold, area distributions depart from power-laws, creating a narrow range of density space over which scale-free area distributions emerge; this would suggest that this mechanism is rare. However, some systems can endogenously maintain themselves near this critical point in a phenomenon referred to as self-organized criticality (Bak et al., 1989). This is accomplished through disturbance processes that propagate via patch contiguity (e.g., forest fires, see Drossel and Schwabl, 1992), maintaining patterns near the percolation threshold through a cycle of large-scale disturbance and slow recovery (Pascual and Guichard, 2005).

Alternatively, power-law scaling of patch areas can arise from the coupled action of local facilitation, which cause patches to expand, and competition for a global resource (e.g., Pascual et al., 2002; Scanlon et al., 2007) that ultimately limits the total density of a given patch type at the landscape scale. In contrast to regular patterning mechanisms, these feedback processes limit landscape-level patch density, but not the size of individual patches, leading to the creation, via local facilitation, of very large patches. This is known as robust criticality because power-law scaling in response can occur over a wide range of external conditions and patch densities, including densities well below the percolation threshold. Robust criticality has been noted in Everglades vegetation distributions (Foti et al., 2012), as well as in a variety of dryland vegetation patterns (Kefi et al., 2011). Widespread occurrence of both local facilitation and global resource competition in ecological systems suggests this process may operate in a multitude of landscapes.

Lastly, we quantified the spectral characteristics (2-dimensional periodicity) of the ridge-slough pattern, which has been described as exhibiting a characteristic wavelength in the direction perpendicular to historical flow (SCT, 2003; Larsen et al., 2007; Watts et al., 2010). Spectral composition is useful for discerning the scale at which spatial feedbacks operate in self-organized systems. This is important because many conceptual models for ridge-slough pattern genesis invoke interactions between spatial feedbacks operating on different characteristic scales. Several models (e.g. Ross et al., 2006; Lago et al., 2010; Cheng et al., 2011) produce distinctly periodic landscapes, which arise from the action of local facilitation feedbacks and, crucially, negative feedbacks on patch expansion that operate at a characteristic scale. For example, evaporative gradients redistribute *P* to local productivity hotspots (ridges) from adjacent source areas (sloughs), but can only do so over a limited range because *P* is ultimately depleted from the source area (Ross et al., 2006; Eppinga et al., 2010). Similarly, sediment transport mechanisms (Larsen et al., 2007; Lago et al., 2010) yield a balance between entrainment and deposition that is governed by focused flow in sloughs, the velocity of which is controlled by the cross-sectional occlusion of flow by ridges. Because patch expansion and contraction is controlled by local heterogeneity in the flow velocity field, this inhibitory feedback operates at a limited spatial scale. Alternatively, feedbacks between hydroperiod and landscape geometry suggested by Cohen et al. (2011), enumerated by Heffernan et al. (2013), and tested at the landscape scale in Kaplan et al. (2012), create a global-scale feedback, and thus invoke no characteristic spatial scale. To that end, we tested the hypothesis that the ridge-slough landscape is regularly patterned (i.e., exhibits a characteristic wavelength), which is consistent with scale-specific negative feedbacks, or whether the landscape lacks periodicity, consistent with scale-free feedbacks.

Taken together, these three aspects of spatial analysis encompass a novel and rigorous set of metrics for the improved quantification of observed and modeled landscape pattern. While developed with a goal of improving pattern descriptions in the Everglades ridge-slough mosaic, this concatenation of metrics may be useful for identifying pattern and discriminating between underlying mechanisms in a diversity of patterned landscapes.

2 Methods

2.1 Vegetation and hydrologic data

We used multiple vegetation maps of the central Everglades, which vary in scale, extent, mapping schemes, and time frame. For all maps, we aggregated vegetation types into binary classes (Table S2 provides the reclassification scheme) of ridges (value = 1) and sloughs (value = 0). Our primary map (M1) was produced by the South Florida Water Management District (SFWMD) using 1 : 24 000-scale color infrared photos from September 1994 (Rutchey, 2005). This map was chosen due to its large, continuous spatial extent and fine mapping detail. The presence of small ($< 25\,\text{m}^2$) landscape features allowed us to rasterize polygons of dominant vegetation at 1 m resolution (i.e., 1 m × 1 m cells). While the presence of small features does not confer map accuracy at that fine scale, it does imply the loss of patch geometric detail with larger cells. Features at this scale can be subject to mapping error and artifacts, likely under-representing their prevalence. As such, patches below $100\,\text{m}^2$ were omitted from patch-level analyses.

We selected 33 6 km × 6 km sites to span the range of current hydrological conditions (i.e., dry in northern areas to wet in southern areas, Fig. 1). We sought to maximize the number of sites with minimal overlap, while avoiding roads and canals. All sites except 20–22 and 32–33 were rotated to align with the prevailing direction of patch elongation (15° counterclockwise).

We used two additional vegetation maps (M2 and M3), which vary in spatial extent, resolution, and sampling date, to corroborate the primary analysis and rule out map resolution effects and temporal changes. M2 was generated from 1 : 24 000 scale aerial photographs taken in 2004 (RECOVER 2014) and rasterized at 50 m resolution. The spatial extent is similar to M1, so the same sites were used (Fig. 2). Although rotation for flow-alignment can induce significant resampling error with larger cells, we found strong agreement between spatial statistics from M2 and an un-rotated version; thus, we used the same rotation scheme for M2 as for M1. The source map for M3 was generated from 1 m resolution digital orthophotos and each site was individually rotated in the direction of elongation (Nungesser, 2011). The spatial extent of the source map was composed of a series of non-adjacent 4 km × 6 km blocks, and correspondingly we chose 10 4 km × 6 km blocks and rasterized at 1 m resolution (Fig. 2). Ridge cells were grouped into patches if they shared at least one edge with an adjacent ridge (i.e., a von Neumann neighborhood).

Within each site, *point-specific* daily average water depths at a grid spacing of 200 m were obtained from the Everglades Depth Estimation Network (EDEN) xyLocator (http://sofia.usgs.gov/eden/edenapps/xylocator.php). We note these water depths are spatially interpolated from a network of water elevation monitoring stations and, as such, represent only an estimate of actual conditions. *Site-specific* mean water depth (MWD) values were obtained by averaging all point-specific values in each site over the period of record from 1991–2010.

2.2 Site-to-site comparisons

Ridge density, edge density, and elongation were compared across sites. Ridge density is the proportion of ridge area to site area, while edge density is the sum of patch perimeters divided by site area. In order to measure elongation, E, we first identify individual lengths and widths (l and w, respectively) as any group of contiguous ridge cells (i.e. unbroken by slough cells) along a row or column. Elongation is the ratio of the mean of these contiguous row and column sections:

$$E = \frac{\frac{1}{n_c}\sum l}{\frac{1}{n_r}\sum w} = \frac{n_r}{n_c} \tag{1}$$

where n_r and n_c represent the number of contiguous row and column sections. Elongation simplifies to the ratio of these since the summation terms both yield the total number of ridge cells. Elongation metrics are highly sensitive to orientation differences between the grid and landscape features. Sites with tortuous flow paths or a poorly aligned grid will underestimate E. As such, we provide estimates of grid orientation alignment with overall feature orientation as a mean patch angle, $\overline{A}_p$, where A_p is the angle between the grid y axis and the major axis of an ellipse with the same second moment as the patch.

Hydrologic trends were identified by regressing MWD against site-level metrics, and were considered statistically significant at $p < 0.05$. For analyses that are highly de-

Title Page
Abstract Introduction
Conclusions References
Tables Figures
◀| |▶
◀ ▶
Back Close
Full Screen / Esc
Printer-friendly Version
Interactive Discussion

pendent on mapping resolution (i.e., total edge), we omit M1 sites north of Interstate-75, as these were mapped using significantly lower resolution than those to the south (Rutchey, 2005). For elongation analyses, we omit sites with ridge densities greater than 0.8, as elongation metrics lose relevance when landscape heterogeneity is minimal.

2.3 Patch size scaling relationships

2.3.1 Patch-geometry scaling

Patch scaling relationships were identified by regressing patch size against patch-level perimeter and elongation. Patch perimeter was the sum of edge cells for a given patch. Patch elongation (Eq. 1), is applied to cells belonging to an individual patch, rather than the landscape as a whole (as for site-site comparisons). We consider patch–scaling relationships statistically significant at $p < 0.05$, and omit sites with less than 100 observations.

2.3.2 Patch size distributions

Patch size scaling properties were evaluated by comparing empirical distributions to several candidate models. Patch size distributions can be described in terms of their complementary cumulative distribution function (CCDF), which gives the probability that the area of an observed patch is greater than or equal to a given area, x. Preliminary analyses showed empirical CCDFs exhibited extremely heavy tails consistent with power-laws (i.e., linear in log-log space), but only above a minimum cutoff, below which patches became less abundant and the CCDF becomes rounded. This form is in relative agreement with both the Generalized Pareto (GP) and truncated lognormal distributions. The GP is given by its CCDF as

$$P(x) = \begin{cases} \left(1 + \frac{k(x-x_{\min})}{\delta}\right)^{-\frac{1}{k}} & \text{for } k \neq 0 \\ \exp\left(-\frac{x-x_{\min}}{\delta}\right) & \text{for } k = 0 \end{cases} \tag{2}$$

for $x \geq x_{\min}$ when $k \geq 0$, and for $x_{\min} \leq x \leq x_{\min} - \delta/k$ when $k < 0$. The GP reduces to the exponential distribution when $k = 0$ and $x_{\min} = 0$ and reduces to a power-law distribution when $k > 0$ an $x_{\min} = \delta/k$. For $k > 0$ and $x_{\min} < \delta/k$ the GP shows exponential-like behavior for low values of x, while the tail asymptotically approaches a power-law for $x \gg x_{\min}$. Within this range of parameters, δ indicates the curvature in the upper end of the distribution (higher values correspond to greater curvature and hence, relatively fewer small patches), while k indicates the scaling properties of the tail, such that for $x \gg x_{\min}$, the power-law scaling exponent α is equivalent to $(1 + 1/k)$ (Pisarenko and Sornette, 2003). Where the GP fits the data well, we can use the estimated parameters as general information about patch size scaling properties.

For the truncated lognormal distribution, the CCDF is defined in terms of the mean ($\mu_{\ln x}$) and SD ($\sigma_{\ln x} > 0$) of $\ln(x)$.

$$P(x) = \frac{\operatorname{erf}\left(\frac{\sqrt{2}\left[\mu_{\ln x} - \ln(x)\right]}{2\sigma_{\ln x}}\right) + 1}{\operatorname{erf}\left(\frac{\sqrt{2}\left[\mu_{\ln x} - \ln(x_{\min})\right]}{2\sigma_{\ln x}}\right) + 1} \qquad x \geq x_{\min} \tag{3}$$

We compared empirical distributions to synthetic data sets created using Monte Carlo simulations ($n = 20\,000$ per model) from the candidate distributions (Clauset et al., 2009). We used a reweighted form of the Kolmogorov–Smirnov (KS) test (Anderson and Darling, 1952):

$$\max_{x \geq x_{\min}} \frac{|S(x) - P(x)|}{\sqrt{P(x)(1 - P(x))}} \tag{4}$$

where $S(x)$ is the empirical CCDF and $P(x)$ is the continuous CCDF of the candidate distribution, fit to the data using maximum likelihood estimation (MLE). In comparing the GP to the lognormal, we were particularly interested in the behavior at the tail end of the distribution, as the lognormal CCDF deviates from a power-law for very large x (Malevergne et al., 2011). The standard KS test is relatively insensitive to tail differences as the CCDF approaches zero; the reweighting scheme remedies this issue.

We compared the candidate distribution fits by generating log-likelihood ratios of modeled distributions and calculating significance values (Clauset et al., 2009). We reject the hypothesis that the empirical data is consistent with a candidate distribution at $p < 0.1$ for the Monte Carlo tests and at $p > 0.1$ for the log-likelihood ratios. The minimum patch size used to create the empirical distributions was chosen to balance between omitting potentially biased values (which may cause us to reject an otherwise valid distribution) and providing a sample size sufficient for accurate parameter estimation. For M1, $x_{\min} = 100\,\mathrm{m}^2$ was chosen. However, this cutoff appeared too low for M3, as that map had significantly fewer patches than predicted by both the GP and lognormal in the 100–500 m^2 range; correspondingly we chose $x_{\min} = 500\,\mathrm{m}^2$ for M3. For both M1 and M3, we omit any sites with fewer than 100 observations.

We note that while the GP is a continuous distribution, raster maps yield discrete data corresponding to the cell size. Where the cells are much smaller than $x_{\min}$, discretization effects are negligible. However, as the cell size approaches $x_{\min}$, discretization can create significant bias. We approximated a discrete version of the GP using the continuous form, assuming that each discrete value represents a continuous data point from $(x - \mathrm{cellsize}/2)$ to $(x + \mathrm{cellsize}/2)$. The corrected $x_{\min}$ value, $x^*_{\min}$, becomes $(x_{\min} - \mathrm{cellsize}/2)$ (e.g., for M1, $x_{\min} = 100\,\mathrm{m}^2$ and $x^*_{\min} = 99.5\,\mathrm{m}^2$). Synthetic data sets were rounded to the nearest discretization level to be consistent. A similar correction for the power-law distribution worked well when $x_{\min}$ was 6-fold larger than the discretization level (i.e., cell size) (Clauset et al., 2009). For maps with a 1 m cell size, $x_{\min}$ was two orders of magnitude greater than the cell size, and we found no significant difference between corrected and uncorrected results. However, for maps with larger cell sizes, discretization effects caused significant error, suggesting the continuous form approximation may not be appropriate. As such, we omitted M2 from patch size distribution analysis.

2.4 Spectral characteristics

Spectral characteristics of the ridge-slough landscape were evaluated from 2-D periodograms generated following the methods of Mugglestone and Renshaw (1998). In brief, we constructed a discrete 2-D Fourier transform (available in most computational software packages) for each binary vegetation map (Kefi et al., 2014), and then took the absolute value to obtain the real number component. The resulting 2-D periodogram (i.e. spectral density) is a grid representing the magnitude of cosine and sine waves of possible wavenumbers (i.e. spatial frequencies), and orientations to the spectrum. Values were averaged across all orientations in equally spaced wavenumber bins to generate radial spectra (r spectra), which indicate the relative spectral density for each corresponding wavenumber bin. Local maxima indicate dominant wavelengths, and thus suggest the presence of spatial periodicity (Couteron, 2002; Kefi et al., 2014), or regular patterning; the absence of local maxima indicates the landscape is aperiodic.

3 Results

3.1 Site-to-site comparisons

3.1.1 Qualitative aspects of the ridge-slough pattern

Visual inspection of the vegetation maps reveals a remarkable range of pattern morphology (Fig. 1). Ridges in northwestern sites (1–5, a) show pronounced striping, which is less apparent in southern sites (18–22, h, i), where ridges appear more elliptical. Eastern sites located below I-75 (5, 9, 13, 14, 17, 28–33, b, f, g, i, j) show fine-scale speckling and disaggregation, with sites 14, 28 and 29 appearing random, with faint outlines of historic pattern.

Individual ridge formations have many small connections between adjacent elongated elements, with larger patches forming web-like morphologies composed of multiple individual elements. Although this behavior is apparent in all sites, it appears to be density dependent, with denser sites often having the majority of the landscape spanned by one large patch (e.g., M1: 2, 5, 8, 9, 11–13, 23–28, 30–33; M2: 1, 2, 4, 5, 8, 9, 12, 23–28, 30–33; M3: a, b, d, j). Within individual sites, large patches are more web-like than smaller ones, which appear more distinctly separated.

3.1.2 Site-based metrics

Ridge density was negatively correlated to MWD (Fig. 2). Deviation from this association was similar across maps and related to geographic position. In particular, ridge densities in the eastern half of the domain (sites 9, 13, 14, 17, 23–33; b, f, g, i, j) were consistently higher than in the western half, suggesting a strong east–west control on density. The correlation between MWD and ridge density increased markedly when sites were partitioned into east and west blocks. Based on recent aerial imagery, low ridge density in site 1 is a misclassification of sparse sawgrass prairies as slough; that site was omitted from regression analyses.

Site-level elongation was also strongly correlated to MWD (Fig. 3). Sites with ridge densities greater than 0.8 show elongation values much lower than this trend. Average patch orientations ($\overline{A}_\mathrm{p}$) indicate consistency between the grid and features (i.e., $\overline{A}_\mathrm{p}$ values close to zero; Table 1). Sites with larger values ($\geq 5^\circ$) of $|\overline{A}_\mathrm{p}|$ (e.g., M1: 1, 22; M2: 9, 18, 25, 27, 29, 31; M3: d, g) may possess underestimated elongation values due to mismatch between patch orientation and map orientation. Also, the anisotropic extent of M3 sites may bias those measurements in favor of higher elongation values compared to sites with square extents (i.e. M1 and M2).

For high resolution maps (M1, M3), edge density was positively correlated to MWD, indicating greater perimeter at deeper sites (Fig. 4a). Moreover, this association shows little influence of ridge density on perimeter, with low ridge density sites often exhibiting significantly higher perimeters than expected by a null model where landscape where cells are randomly occupied. For M2, in contrast, the relationship is consistent with such a null model, where edge density is maximized when occupied cells reach a density of 0.5, and smoothly declines to zero as density approaches zero or one (Gardner et al., 1987). This pattern is clear for M2 (Fig. 4b), suggesting ridge density alone controls perimeter values, not an underlying hydrologic phenomenon. Notably, when M1 was resampled to 50 m cells, perimeter was strongly controlled by ridge density. This discrepancy between low- and high-resolution maps suggests that the MWD vs. perimeter relationship is manifest principally as variation in fine-scale geometry.

3.2 Patch size scaling relationships

3.2.1 Patch-geometry scaling

For all maps, a significant positive association between patch elongation and patch size was observed in most sites (p values in Table 1), indicating that patches become more elongated with size (Fig. 5b). Likewise, the association between patch perimeter and area was inconsistent with a fractal relationship. All sites were better approximated (F statistic < 0.001) by quadratic rather than linear perimeter-to-area scaling on log-log plots (Fig. 5a), indicating larger patches have higher perimeters than expected from a fractal relationship.

3.2.2 Patch size distributions

Patch area distributions were consistent with the Generalized Pareto distribution (Fig. 6), with 16 of 25 sites passing GP Monte Carlo tests for M1 and 4 of 9 passing for M3 (Table S1). Several sites that were not significant contained extremely large patches, but had little deviation in the rest of the distribution; in some cases (e.g., sites 2, 5, 8, 9, 11, 12, 13, 28, 31; a, d, j) the largest patch was over an order of magnitude larger than predicted based on the GP distribution. All these sites with extremely large patches have ridge densities above or very close to the percolation threshold of a square lattice (~ 0.59, Stauffer, 1995). Above this percolation threshold, the largest patch becomes "over-connected", suggesting that failure of Monte Carlo tests within this group may be density driven, rather than a result of an underlying patterning mechanism. Note that these sites are largely located in the north and eastern sections of the study area, a region typified by high ridge densities. The log-normal distribution was significant in only 4 of 25 sites for M1 and 2 of 9 sites for M3. Although these sites (15, 16, 19, 21; c and h) showed slight rounding in the extreme tail, log-likelihood ratios were not different enough to distinguish between the two candidate distributions (Table S1).

Within each map, GP parameters were remarkably consistent across sites, with almost constant estimates of k and δ for sites that passed Monte Carlo tests (Table S1). Area scaling in the tail of the distribution is illustrated by the $1+1/k$ (analogous to the scaling exponent of a power-law distribution) $= 1.77 \pm 0.06$ for M1 and 1.87 ± 0.13 for M3. The δ parameter indicates how sharply the head of the distribution deviates from a power-law, with larger values indicating that smaller patch areas become exceedingly rare. For M1 and M3, $\delta = 474 \pm 88$ and 1490 ± 219; these differences are likely due to map resolution, with M3 under-representing smaller patches. This is also apparent in sites 1 and 2, which were mapped at lower resolution than the rest of M1, and show higher δ values.

3.3 Spectral characteristics

Spatial periodogram analysis showed no evidence of periodicity. The absence of peak values other than the smallest wavenumber indicates that there is no dominant pattern wavelength, a finding consistent across hydrologic conditions and morphologies (Fig. 5c). Spearman correlations show the r spectra were monotonically decreasing across sites (Rho values in Table 1), a finding consistent with spatial variation that is maximum at the largest scale and decreases consistently towards smaller scales. Furthermore, the form of the r spectra is approximately linear in log-log space suggesting an inverse power–law relationship, consistent with $1/f$ noise (Bak et al., 1989). Some rounding at the lower and upper extremes suggest white noise. For low wavenumbers this is consistent with finite size effects arising from limited sampling domain. Very deep sites (e.g. 9, 13, 14, 17, 18, 19, 22, 28, 29) show a slightly more rounded r spectra than expected from $1/f$ noise, with relatively greater densities of high to medium wavenumbers, but still clearly lack any significant indication of periodicity.

4 Discussion

4.1 Site-to-site comparisons

Site-to-site comparisons highlight a significant connection between inundation (i.e., mean water depth, MWD) and ridge-slough patterning. In terms of landscape composition, the decline in ridge abundance with MWD is consistent with conceptual models that predict that changes in water levels precipitate transitions between ridge and slough by modifying production and respiration dynamics (Givnish et al., 2008; Watts et al., 2010) and inducing state changes (Zweig et al., 2008). The implication that these dynamics differ in eastern and western sections of the study area was unexpected, and points to unexplained controls on ridge expansion. The largest difference between the east and west trends occurs at low water depths, indicating that this control is most pronounced in drier sites. In short, the deviation seen in eastern sites represents a shifting of the relationship to favor sawgrass expansion in extremely dry sites, rather than a general reduction of the hydrologic limitation (since deep sites remain the least affected).

A strong relationship between MWD and key indicators of the shape of the ridge-slough pattern was also observed. Arguably the most salient feature of the pattern, elongation, showed strong dependence on MWD, with maximum elongation observed at low to intermediate water depths. This suggests that ridge features fragment into smaller, less elongated patches under deeper water conditions, a finding previously observed anecdotally (McVoy et al., 2011) and in the spatial statistics of soil elevation (Watts et al., 2010). Although perimeter values relate to several aspects of landscape geometry (e.g. patch complexity, aggregation), the positive correlation with depth further supports the presence of a depth-dependent fragmentation process.

4.2 Patch size scaling relationships

4.2.1 Patch size distributions

Despite the rounding behavior at low-end of the distributions, patch sizes are consistent with scale-free behavior (i.e. power-laws), as power-law distributions are only valid above some minimum value, since they diverge as area approaches zero. However, the higher δ values in data sets with lower resolutions (i.e. M3 and sites north of I-75 in M1) indicate that rounding at the low-end of the distribution may result from under-representation of small features due to mapping resolution. Visual inspection of recent and historical aerial imagery supports this suggestion.

Although power-law scaling can be produced via a wide range of phenomena (Newman et al., 2005), other information about the ridge-slough system can be used to rule out some mechanisms. Power-law scaling of patch areas that arises from the system being near the percolation threshold (i.e., at criticality) occur within a relatively narrow region of parameter space. However, observed power-law scaling in patch areas across a wide range of environmental conditions suggests robustness in the phenomena inconsistent with these processes. Our findings comport with those of Foti et al. (2012) who observed similar scaling behavior over a wide range of vegetation types and densities. Self-organized criticality is capable of producing power-law scaling at varying densities, but requires strong temporal variation in ridge density as the system endogenously readjusts towards criticality following disturbances (Pascual and Guichard, 2005). However, a recent paleoecological study (Bernhardt and Willard, 2010) suggests that ridge-slough configurations and densities have remained relatively stable since their initial formation. Likewise, we are aware of no documented disturbance regime that exhibits the characteristic strong separation of time scales associated with self-organized criticality. While peat fires might be invoked, evidence for widespread incidence and large-scale impacts of these prior to hydrologic modification is not present (McVoy et al., 2011). Robust criticality provides an explanation that does not require a disturbance and recovery regime operating on widely divergent time scales, or the requisite temporal dynamics in ridge density necessary to invoke self-organized criticality. Rather, power-law scaling across a wide range of parameter space, as well as the presence of ridge densities that smoothly vary along environmental gradients is consistent with robust criticality, wherein local facilitative processes induce clustering while a global limitation maintains landscape heterogeneity (Pascual and Guichard, 2005).

4.2.2 Patch-geometry scaling

Although patch area distributions indicate scale invariance, other geometric properties show scale dependence with patch size. Patch elongation was shown to increase with patch size, indicating that patches are not strictly self-similar. Although the patch elongation scaling may result from scale-dependent mechanisms (i.e., processes that impose a characteristic spatial scale) it may also suggest anisotropic scale-free processes that produce self-affinity, a fractal form where geometric features scale via separate relations in the x and y directions. Self-affinity implies that lengths and widths are scale invariant with respect to their orthogonal directions, however the patches as a whole only become scale invariant when an anisotropic rescaling transformation is made (Sapozhnikov and Foufoula-Georgiou, 1996).

Patch perimeter also shows departure from fractal scaling, with patches increasing in perimeter more rapidly with size than expected from a simple fractal relationship. The mechanisms driving this are unclear. Multiple processes can induce large patches to form greater than expected perimeters, such as the increased elongation, web-like connectivity, or increased crenulation. Conversely, this curvature may be due to artifacts such as the mapping scheme capturing a greater proportion of the relative detail for larger patches relative to small patches. Resolution limitations become more apparent on small-scale features when mapped at the same resolution as large scale features. Detail-sensitive measurements like perimeter may be skewed according to relative patch scale such that, at low-resolution, small patches are represented as more Euclidean shapes (i.e. having boxier edges), while larger patches retain more complex representations, creating artificial scale dependence. However, while inference of intrinsic perimeter scaling relations may be problematic because of these map resolution effects, this effect is unlikely to explain variation in patch elongation with patch size because small patches are free to achieve very high elongation values (e.g. the cutoff patch size for M1 of 100 m^2 is capable of producing elongation values up to 100, well above any observed value).

4.2.3 Spectral characteristics

The ridge-slough pattern is extensively referenced as periodic (SCT 2003; Wetzel et al., 2005; Ross et al., 2006; Larsen, 2007; Givnish et al., 2008; Larsen and Harvey, 2010; Lago et al., 2010; Watts et al., 2010; Cheng et al., 2011; Nungesser, 2011; Heffernan et al., 2013; Sullivan et al., 2014). Correspondingly, the strong support against spatial periodicity from the 2-D periodograms is particularly interesting and relevant. The pattern, which has qualitatively been interpreted as regular bands of sawgrass, consistently lacks any indication of periodic spectral structure (i.e. peaks in r spectrum). This aperiodicity suggests the absence of significant long-range negative feedbacks (Rietkerk and Van de Koppel, 2008), ruling out many of the mechanisms invoked to explain regular pattern formation (Borgogno et al., 2009). Indeed, the flow-parallel directionality of the bands is also a departure from periodic configurations in other settings, where most vegetation bands in periodic systems are elongated in the direction perpendicular to environmental anisotropy (Rietkerk et al., 2002). In short, this result suggests that the mechanisms responsible for ridge-slough landscape geometry are not scale-dependent negative feedbacks that are the driver of regular patterns.

Furthermore, power-law behavior in patch area distributions are inconsistent with regular patterning. Model realizations show periodic landscapes possess patch area distributions that appear Gaussian, with distinct peaks corresponding to the characteristic patch size (von Hardenberg, 2010; Kefi et al., 2014). In sharp contrast, the scale-free landscapes, which are implied by power-law distributions of area, do not show a characteristic value (i.e., mode), but rather show the absence of any dominant size.

4.2.4 Synthesis of landscape characteristics

As one mechanism that may underlie the emergence of scale-free landscape pattern geometry, robust criticality suggests the presence of both local facilitation and global limitation mechanisms. Locally facilitative effects are almost certainly present in the Everglades, given the tight aggregation of patches observed in many parts of the landscape. Local facilitation may take the form of autogenic peat accretion (Larsen et al., 2007), clonal propagation of sawgrass (Brewer, 1996), nutrient accumulation on ridges (Cohen et al., 2009), or local seed dispersal, although the relative importance and directionality of these mechanisms remains unknown (Acharya et al., 2015). Likewise, several limiting processes exist in the ridge slough landscape, however, their associated dynamics can be used to identify those capable of producing scale-free phenomena.

Recent modeling studies (Manor and Shnerb, 2008a; von Hardenberg, 2010) suggest that a key distinction between limiting processes that produce periodic and scale-free patterning is the nature of the diffusivity of the limiting source, or the spatial scale over which that limiting feedback occurs. Specifically, when the limiting process has high diffusivity (i.e., spatially equilibrates quickly in response to demand), the magnitude of the effect remains relatively constant across the landscape, and is therefore considered global. Under this condition, there is no inherent limit to how large a patch can grow relative to other patches, as the negative feedback to expansion is exerted equally on all areas of the landscape, regardless of spatial configuration. Conversely, when the limiting process diffusivity is low, its influence is spatially constrained by an effective diffusive length. Under these conditions, patches cannot continue to expand, and the landscape self-organizes into a periodic configuration.

Although the ecosystems of the Everglades are highly phosphorus limited (Noe et al., 2001), strong nutrient gradients have been shown between ridge and slough communities (Ross et al., 2006) as well as between tree-island and marsh communities (Wetzel et al., 2009), indicating slow diffusivity relative to nutrient uptake. As a consequence, were this the dominant control on pattern formation, the range of individual patch expansion would be limited, forming regular patterning. As demonstrated by our observations of site-to-site variation, as well as numerous other studies (e.g., Givnish et al., 2008; Zwieg and Kitchens, 2008; Todd et al., 2012), ridges are also limited by water depths. As ridges, which act to displace water and, more importantly occlude flow, expand into low elevation sloughs, they cause regional water levels to increase, creating a negative feedback that limits ridge density (Kaplan et al., 2012). Because water depths equilibrate quickly, they are consistent with the high diffusivity required for the global feedback that would lead to emergence of scale free pattern. As this limitation becomes less pronounced (e.g., in drier sites), ridge density approached unity, and landscape heterogeneity is lost. Correspondingly, water depths emerge as a strong candidate for a global feedback necessary for pattern formation.

Finally, we note that the nature of the anisotropy in the landscape is particularly interesting, given that visually compelling banding as is observed in the Everglades is not typically observed in scale-free patterning. The finding that elongated landscape features do not impose periodicity suggests that a wide range of spatial structures (in ecological systems and elsewhere) may have been misclassified as regularly patterned, either due to the lack of robust methods (i.e., periodogram analysis), or misinterpretation of results. In short, aperiodic banding may be more prevalent than the literature suggests. As a specific generation mechanism for aperiodic banding, Acharya et al. (2015)

recently showed that by introducing anisotropy into the local facilitation kernel of a robust criticality model, one can produce directional banding without imposing periodicity, yielding simulated landscape patterns that show high statistical and visual fidelity to the patterns observed in the ridge-slough landscape. The dynamics of such a system are relatively unexplored, and warrant further examination.

The Supplement related to this article is available online at doi:10.5194/hessd-12-2975-2015-supplement.

Acknowledgements. We gratefully acknowledge the funding support from the US Army Corps of Engineers via the Cooperative Ecosystem Studies Unit (CESU) and the Monitoring and Assessment Plan (MAP) (Contract Agreement #12-2-0011).

References

Acharya, S., Kaplan, D. A., Casey, S., Cohen, M. J., and Jawitz, J. W.: Coupled local facilitation and global hydrologic inhibition drive landscape geometry in a patterned peatland, Hydrol. Earth Syst. Sci. Discuss., 12, 1247–1277, doi:10.5194/hessd-12-1247-2015, 2015.

Anderson, T. W. and Darling, D. A.: Asymptotic theory of certain “goodness of fit” criteria based on stochastic processes, Ann. Math. Stat., 23, 193–212, 1952.

Bak, P., Tang, C., and Wiesenfeld, K.: Self-organized criticality, Phys. Rev. A, 38, 364–374, doi:10.1103/PhysRevA.38.364, 1989.

Borgogno, F., D’Odorico, P., Laio, F., and Ridolfi, L.: Mathematical models of vegetation pattern formation in ecohydrology, Rev. Geophys., 47, RG1005, doi:10.1029/2007RG000256, 2009.

Brewer, J. S.: Site differences in the clone structure of an emergent sedge, Cladium jamaicense, Aquat. Bot., 55, 79–91, doi:10.1016/S0304-3770(96)01060-1, 1996.

Cheng, Y., Stieglitz, M., Turk, G., and Engel, V.: Effects of anisotropy on pattern formation in wetland ecosystems, Geophys. Res. Lett., 38, L04402, doi:10.1029/2010GL046091, 2011.

Clauset, A., Shalizi, C. R., and Newman, M. E.: Power-law distributions in empirical data, SIAM Rev., 51, 661–703, doi:10.1137/070710111, 2009.

Cohen, M. J., Osborne, T. Z., Lamsal, S. J., and Clark, M. W.: Regional Distribution of Soil Nutrients-Hierarchical Soil Nutrient Mapping for Improved Ecosystem Change Detection, South Florida Water Management District, West Palm Beach, Florida, USA, 91 pp., 2009.

Couteron, P.: Quantifying change in patterned semi-arid vegetation by Fourier analysis of digitized aerial photographs, Int. J. Remote Sens., 23, 3407–3425, doi:10.1080/01431160110107699, 2002.

Eppinga, M. B., Rietkerk, M., Borren, W., Lapshina, E., Bleuten, W., and Wassen, M.: Regular surface patterning of peatlands: confronting theory with field data, Ecosystems, 11, 520–536, doi:10.1007/s10021-008-9138-z, 2008.

Foti, R., del Jesus, M., Rinaldo, A., and Rodriguez-Iturbe, I.: Hydroperiod regime controls the organization of plant species in wetlands, P. Natl. Acad. Sci. USA, 109, 19596–19600, doi:10.1073/pnas.1218056109, 2012.

Gardner, R. H., Milne, B. T., Turner, M. G., and O'Neill, R. V.: Neutral models for the analysis of broad-scale landscape pattern, Landscape Ecol., 1, 19–28, doi:10.1007/BF02275262, 1987.

Givnish, T. J., Volin, J. C., Owen, V. D., Volin, V. C., Muss, J. D., and Glaser, P. H.: Vegetation differentiation in the patterned landscape of the central Everglades: importance of local and landscape drivers, Global Ecol. Biogeogr., 17, 384–402, doi:10.1111/j.1466-8238.2007.00371.x, 2008.

Heffernan, J. B., Watts, D. L., and Cohen, M. J.: Discharge competence and pattern formation in peatlands: a meta-ecosystem model of the everglades ridge-slough landscape, PloS one, 8, e64174, doi:10.1371/journal.pone.0064174, 2013.

Kaplan, D. A., Paudel, R., Cohen, M. J., and Jawitz, J. W.: Orientation matters: patch anisotropy controls discharge competence and hydroperiod in a patterned peatland, Geophys. Res. Lett., 39, L17401, doi:10.1029/2012GL052754, 2012.

Kéfi, S., Rietkerk, M., Alados, C. L., Pueyo, Y., Papanastasis, V. P., ElAich, A., and De Ruiter, P. C.: Spatial vegetation patterns and imminent desertification in Mediterranean arid ecosystems, Nature, 449, 213–217, doi:10.1038/nature06111, 2007.

Kéfi, S., Rietkerk, M., Roy, M., Franc, A., De Ruiter, P. C., and Pascual, M.: Robust scaling in ecosystems and the meltdown of patch size distributions before extinction, Ecol. Lett., 14, 29–35, doi:10.1111/j.1461-0248.2010.01553.x, 2011.

Kéfi, S., Guttal, V., Brock, W. A., Carpenter, S. R., Ellison, A. M., Livina, V. N., Seekell, D. A., Scheffer, M., van Nes, E. H., and Dakos, V.: Early warning signals of ecological transitions: methods for spatial patterns, PloS one, 9, e92097, doi:10.1371/journal.pone.0092097, 2014.

Lago, M. E., Miralles-Wilhelm, F., Mahmoudi, M., and Engel, V.: Numerical modeling of the effects of water flow, sediment transport and vegetation growth on the spatiotemporal patterning of the ridge and slough landscape of the Everglades wetland, Adv. Water Resour., 33, 1268–1278, doi:10.1016/j.advwatres.2010.07.009, 2010.

Larsen, L. G. and Harvey, J. W.: How vegetation and sediment transport feedbacks drive landscape change in the Everglades and wetlands worldwide, Am. Nat., 176, E66–E79, 2010.

Larsen, L. G., Harvey, J. W., and Crimaldi, J. P.: A delicate balance: ecohydrological feedbacks governing landscape morphology in a lotic peatland, Ecol. Monogr., 77, 591–614, doi:10.1890/06-1267.1, 2007.

Larsen, L. G., Aumen, N., Bernhardt, C., Engel, V., Givnish, T., Hagerthey, S., Harvey, J., Leonard, L., McCormick, P., McVoy, C., Noe, G., Nungesser, M., Rutchey, K., Sklar, F., Troxler, T., Volin, J., and Willard, D.: Recent and historic drivers of landscape change in the Everglades ridge, slough, and tree island mosaic, Crit. Rev. Env. Sci. Tec., 41, 344–381, doi:10.1080/10643389.2010.531219, 2011.

Li, H. and Wu, J.: Use and misuse of landscape indices, Landscape Ecol., 19, 389–399, doi:10.1023/B:LAND.0000030441.15628.d6, 2004.

Light, S. S. and Dineen, J. W.: Water Control in the Everglades: a Historical Perspective, Everglades: the Ecosystem and its Restoration, St. Lucie Press, Delray Beach, Florida, 47–84, 1994.

Limpert, E., Stahel, W. A., and Abbt, M.: Log-normal distributions across the sciences: keys and clues, Bioscience, 51, 341–352, doi:10.1641/0006-3568(2001)051[0341:LNDATS]2.0.CO;2, 2001.

Lovejoy, S.: Area-perimeter relation for rain and cloud areas, Science, 216, 185–187, doi:10.1126/science.216.4542.185, 1982.

Ludwig, J. A., Tongway, D. J., and Marsden, S. G.: Stripes, strands, or stipples: modelling the influence of three landscape banding patterns on resource capture and productivity in semi-arid woodlands, Australia, Catena, 37, 257–273, doi:10.1016/S0341-8162(98)00067-8, 1999.

Malevergne, Y., Pisarenko, V., and Sornette, D.: Testing the Pareto against the lognormal distributions with the uniformly most powerful unbiased test applied to the distribution of cities, Phys. Rev. E, 83, 036111, doi:10.1103/PhysRevE.83.036111, 2011. (FOUND!)

Mandelbrot, B. B.: The Fractal Geometry of Nature, Freeman, New York, 1983.

Manor, A. and Shnerb, N. M.: Facilitation, competition, and vegetation patchiness: from scale free distribution to patterns, J. Theor. Biol., 253, 838–842, doi:10.1016/j.jtbi.2008.04.012, 2008a.

Manor, A. and Shnerb, N. M.: Origin of Pareto-like spatial distributions in ecosystems, Phys. Rev. Lett., 101, 268104, doi:10.1103/PhysRevLett.101.268104, 2008b.

McVoy, C., Park Said, W., Obeysekera, J., VanArman, J., and Dreschel, T.: Landscapes and Hydrology of the Predrainage Everglades, University Press of Florida, Gainesville, FL, 2011.

Mugglestone, M. A. and Renshaw, E.: Detection of geological lineations on aerial photographs using two-dimensional spectral analysis, Comput. Geosci., 24, 771–784, doi:10.1016/S0098-3004(98)00065-X, 1998.

Newman, M. E.: Power laws, Pareto distributions and Zipf's law, Contemp. Phys., 46, 323–351, doi:10.1080/00107510500052444, 2005.

Noe, G. B., Childers, D. L., and Jones, R. D.: Phosphorus biogeochemistry and the impact of phosphorus enrichment: why is the Everglades so unique?, Ecosystems, 4, 603–624, doi:10.1007/s10021-001-0032-1, 2001.

Nungesser, M. K.: Reading the landscape: temporal and spatial changes in a patterned peatland, Wetl. Ecol. Manag., 19, 475–493, doi:10.1007/s11273-011-9229-z, 2011.

Pascual, M. and Guichard, F.: Criticality and disturbance in spatial ecological systems, Trends Ecol. Evol., 20, 88–95, doi:10.1016/j.tree.2004.11.012, 2005.

Pascual, M., Roy, M., Guichard, F., and Flierl, G.: Cluster size distributions: signatures of self–organization in spatial ecologies, Philos. T. R. Soc. B, 357, 657–666, doi:10.1098/rstb.2001.0983, 2002.

Pickett, S. T. and Cadenasso, M. L.: Landscape ecology: spatial heterogeneity in ecological systems, Science, 269, 331–334, doi:10.1126/science.269.5222.331, 1995.

Pisarenko, V. F. and Sornette, D.: Characterization of the frequency of extreme earthquake events by the generalized Pareto distribution, Pure Appl. Geophys., 160, 2343–2364, doi:10.1007/s00024-003-2397-x, 2003.

RECOVER: 2014 System Status Report, Restoration Coordination and Verification Program, c/o US Army Corps of Engineers, Jacksonville, FL, and South Florida Water Management District, West Palm Beach, FL, 2014.

Remmel, T. K. and Csillag, F.: When are two landscape pattern indices significantly different?, J. Geogr. Syst., 5, 331–351, doi:10.1007/s10109-003-0116-x, 2003.

Rietkerk, M. and Van de Koppel, J.: Regular pattern formation in real ecosystems, Trends Ecol. Evol., 23, 169–175, doi:10.1016/j.tree.2007.10.013, 2008.

Ross, M. S., Mitchell-Bruker, S., Sah, J. P., Stothoff, S., Ruiz, P. L., Reed, D. L., Jayachandran, K., and Coultas, C. L.: Interaction of hydrology and nutrient limitation in the Ridge and Slough landscape of the southern Everglades, Hydrobiologia, 569, 37–59, doi:10.1007/s10750-006-0121-4, 2006.

Rutchey, K., Vilchek, L., and Love, M.: Development of a vegetation map for Water Conservation Area 3, Technical Publication ERA Number 421, South Florida Water Management District, West Palm Beach, FL, USA, 2005.

Sapozhnikov, V. and Foufoula-Georgiou, E.: Self-affinity in braided rivers, Water Resour. Res., 32, 1429–1439, doi:10.1029/96WR00490, 1996.

Science Coordination Team: The Role of Flow in the Everglades Ridge and Slough Landscape, South Florida Ecosystem Restoration Working Group, West Palm Beach, FL, 2003.

Stauffer, D. and Aharony, A.: Introduction to percolation theory, Taylor and Francis, London, 1991.

Sullivan, P. L., Price, R. M., Miralles-Wilhelm, F., Ross, M. S., Scinto, L. J., Dreschel, T. W., Sklar, F. H., and Cline, E.: The role of recharge and evapotranspiration as hydraulic drivers of ion concentrations in shallow groundwater on Everglades tree islands, Florida (USA), Hydrol. Process., 28, 293–304, doi:10.1002/hyp.9575, 2014.

Todd, M. J., Muneepeerakul, R., Pumo, D., Azaele, S., Miralles-Wilhelm, F., Rinaldo, A., and Rodriguez-Iturbe, I.: Hydrological drivers of wetland vegetation community distribution within Everglades National Park, Florida, Adv. Water Resour., 33, 1279–1289, 2010.

Turner, M. G.: Landscape Ecology in Theory and Practice: Pattern and Process, Springer-Verlag, New York, 2001.

Turner, M. G.: Landscape ecology: what is the state of the science?, Annu. Rev. Ecol. Evol. S., 36, 319–344, doi:10.1146/annurev.ecolsys.36.102003.152614, 2005.

von Hardenberg, J., Kletter, A. Y., Yizhaq, H., Nathan, J., and Meron, E.: Periodic vs. scale-free patterns in dryland vegetation, P. R. Soc. B, 277, 1771–1776, doi:10.1098/rspb.2009.2208, 2010.

Watts, D. L., Cohen, M. J., Heffernan, J. B., and Osborne, T. Z.: Hydrologic modification and the loss of self-organized patterning in the ridge–slough mosaic of the Everglades, Ecosystems, 13, 813–827, doi:10.1007/s10021-010-9356-z, 2010.

Weerman, E. J., Van Belzen, J., Rietkerk, M., Temmerman, S., Kéfi, S., Herman, P. M. J., and de Koppel, J. V.: Changes in diatom patch-size distribution and degradation in a spatially self-organized intertidal mudflat ecosystem, Ecology, 93, 608–618, doi:10.1890/11-0625.1, 2012.

Wetzel, P. R., van der Valk, A. G., Newman, S., Gawlik, D. E., Troxler Gann, T., Coronado-Molina, C. A., Childers, D. L., and Sklar, F. H.: Maintaining tree islands in the Florida Everglades: nutrient redistribution is the key, Front. Ecol. Environ., 3, 370–376, doi:10.1890/1540-9295(2005)003[0370:MTIITF]2.0.CO;2, 2005.

Wetzel, P. R., van der Valk, A. G., Newman, S., Coronado, C. A., Troxler-Gann, T. G., Childers, D. L., Orem, W. H., and Sklar, F. H.: Heterogeneity of phosphorus distribution in a patterned landscape, the Florida Everglades, Plant Ecol., 200, 83–90, doi:10.1007/s11258-008-9449-3, 2009.

Wu, Y., Wang, N., Rutchey, K.: An analysis of spatial complexity of ridge and slough patterns in the Everglades ecosystem, Ecol. Complex., 3, 183–192, doi:10.1016/j.ecocom.2005.12.002, 2006.

Yuan, J., Cohen, M. J., Kaplan, D. A., Acharya, S., Larsen, L. G., and Nungesser, M. K.: Linking metrics of landscape pattern to hydrological process in a lotic wetland, Landscape Ecol., in review, 2015.

Zweig, C. L. and Kitchens, W. M.: Effects of landscape gradients on wetland vegetation communities: information for large-scale restoration, Wetlands, 28, 1086–1096, doi:10.1672/08-96.1, 2008.

Table 1. Selected site properties for all maps (M1, M2, M3). Mean patch angle (A_p) measures the angle difference between patch and site orientation. The p value for patch $L:W$ indicates the significance of a linear regression relating patch length-to-width to area. Rho, a Spearman correlation, indicates the monotonicity of observed r spectrum plots with a value of 1 corresponding to a perfectly monotonic function; Rho values were > 0.999 for all sites in M1 and M3 confirming the absence of a characteristic pattern wavelength. NA values correspond to sites that were omitted from patch-level analyses because they contained less than 100 patches.

M1			M2				M3		
Site	A_p (deg)	Patch $L:W$ (p value)	Site	A_p (deg)	Patch $L:W$ (p value)	r spectrum Rho	Site	A_p (deg)	Patch $L:W$ (p value)
1	−5.7	0.13	1	−0.50	0.00	0.974	a	2.8	0.00
2	1.8	0.05	2	−0.40	0.00	0.981	b	NA	NA
3	2.7	0.00	3	4.50	0.00	0.979	c	1.2	0.00
4	−1.2	0.00	4	0.20	0.00	0.972	d	−7.2	0.00
5	−3.9	0.00	5	3.60	0.00	0.982	e	0.7	0.01
6	0.9	0.00	6	2.30	0.00	0.978	f	−0.7	0.00
7	−2.4	0.00	7	0.60	0.00	0.986	g	−5.0	0.01
8	−3.6	0.00	8	2.00	0.00	0.980	h	−1.4	0.00
9	−2.2	0.32	9	8.50	0.01	0.964	i	3.2	0.00
10	−1.5	0.00	10	2.60	0.00	0.964	j	−3.3	0.03
11	0.4	0.00	11	2.70	0.00	0.973			
12	−3.8	0.00	12	0.50	0.00	0.979			
13	0.5	0.21	13	2.00	0.00	0.971			
14	−0.3	0.00	14	4.10	0.00	0.961			
15	−4.5	0.00	15	2.60	0.00	0.977			
16	−3.1	0.00	16	0.90	0.00	0.973			
17	−0.1	0.00	17	1.20	0.00	0.970			
18	−2.7	0.00	18	5.20	0.00	0.975			
19	−4.0	0.00	19	0.80	0.00	0.960			
20	−4.0	0.00	20	−1.50	0.00	0.986			
21	2.5	0.00	21	1.00	0.00	0.980			
22	−6.4	0.00	22	0.30	0.00	0.977			
23	NA	NA	23	NA	NA	0.976			
24	NA	NA	24	NA	NA	0.943			
25	NA	NA	25	14.70	0.35	0.968			
26	NA	NA	26	NA	NA	0.954			
27	NA	NA	27	5.30	0.57	0.976			
28	−2.6	0.33	28	2.70	0.00	0.982			
29	−2.3	0.10	29	5.00	0.00	0.964			
30	NA	NA	30	NA	NA	0.952			
31	3.1	0.09	31	5.10	0.31	0.969			
32	NA	NA	32	NA	NA	0.969			
33	NA	NA	33	−3.30	0.49	0.965			

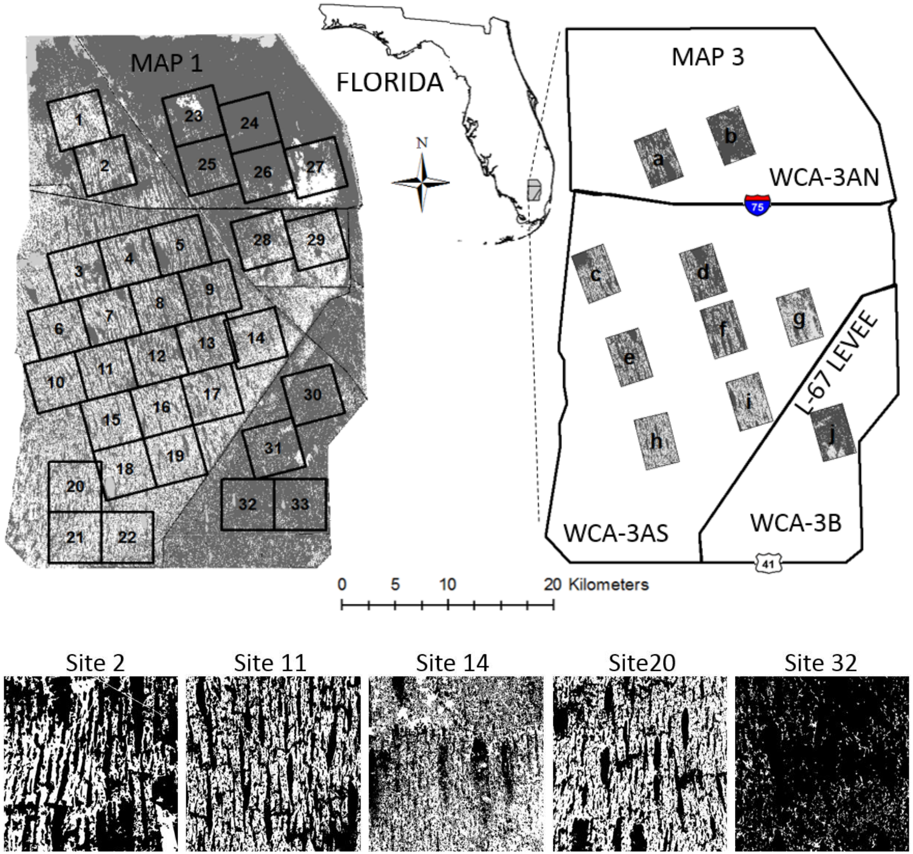

Figure 1. Study area and site locations (including major roads, hydrologic compartments, and levees) for the primary map (M1; numbered sites), and the secondary map (M3; lettered sites). Another map (M2; not shown) has same domain as M1, but lower pixel resolution (50 m vs. 1 m). Sites spanning the pattern gradient in WCA3 are shown below.

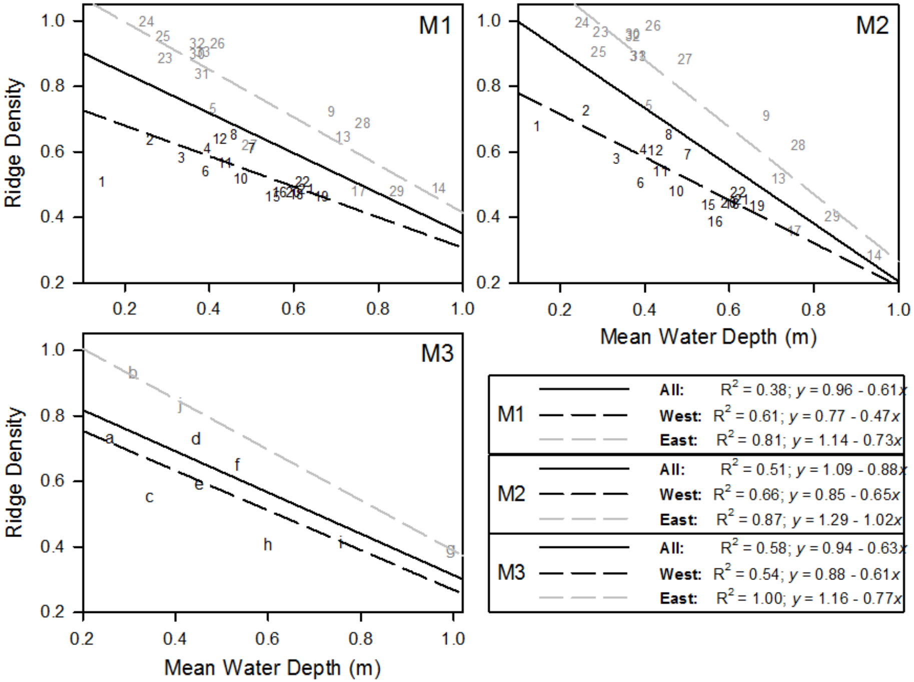

Figure 2. Ridge density is limited by mean water depth. Across maps, ridge density is negatively correlated to mean water depth. Although the relationship is linear (dashed line), there is consistent east vs. west deviation from this relationship. Eastern sites (denoted in grey) show consistently higher ridge densities than those in the west. Trends associated with east–west segregation (dotted lines) show much stronger relationships than the composite trend (solid line). Site 1 was omitted due to possible misclassification.

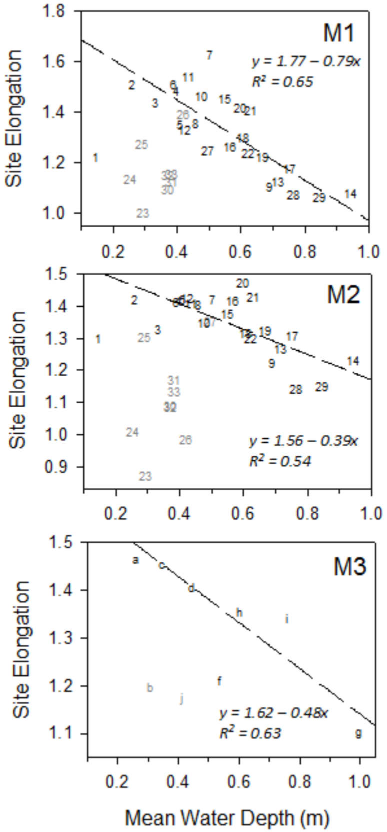

Figure 3. Site elongation shows a strong dependence on mean water depth. Sites with ridge densities greater than 0.8 (indicated in grey) were omitted from regressions and show elongation values lower than expected from this trend. Site 1 was omitted due to possible misclassification issues.

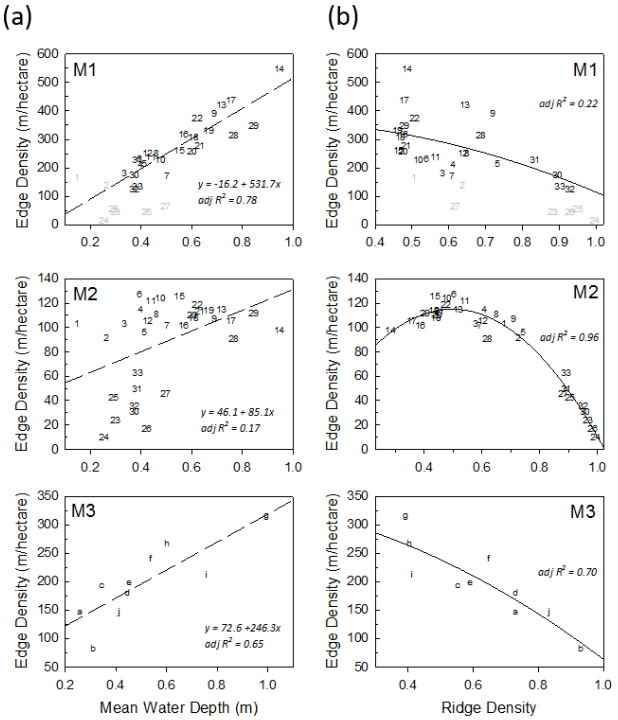

Figure 4. (a) Edge density is positively correlated to mean water depth. Higher edge densities in deeper sites is consistent with patches becoming disaggregated with increased water depth. Gray sites in M1 indicate those mapped at lower resolution, and omitted from regressions. **(b)** If edge density is unaffected by depth, we would predict a peak in edge density when ridge and slough heterogeneity is maximized (i.e., ridge density = 0.5) and a minimum when heterogeneity is minimized (i.e., ridge density = 0 or 1). M2 is consistent with the hypothesis, while M1 and M3 show deviation from this trend. When M1 was resampled to 50 m pixels (not shown), the relationship was congruent with M2, indicating that larger pixel sizes do not to capture the scale of features responsible for this correlation.

Title Page
Abstract | Introduction
Conclusions | References
Tables | Figures
◀| |▶
◀ ▶
Back | Close
Full Screen / Esc
Printer-friendly Version
Interactive Discussion

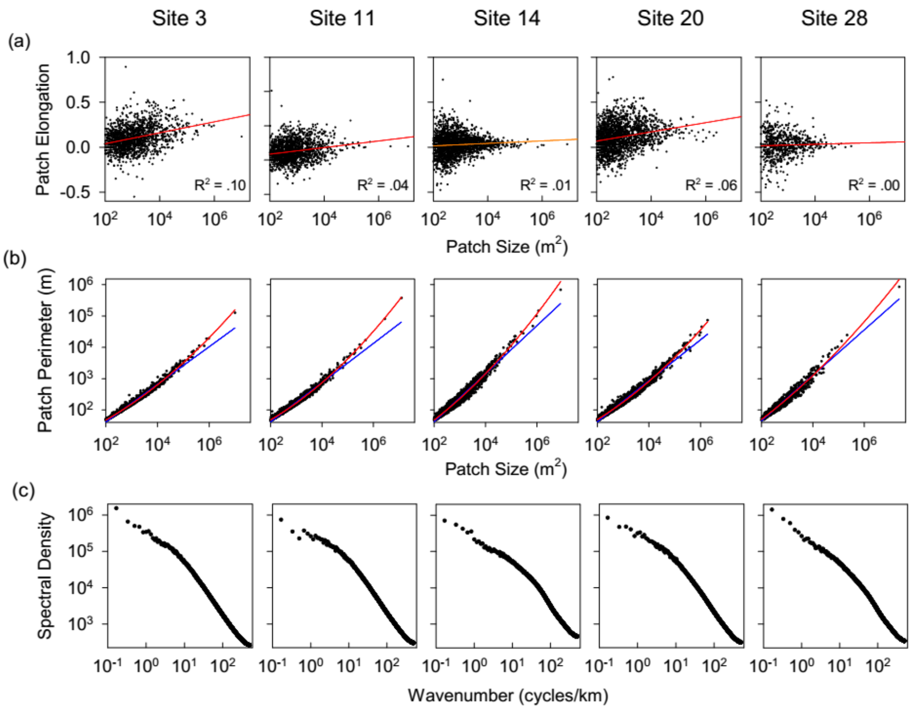

Figure 5. Selected site characteristics across a range of hydrologic conditions. **(a)** Patch elongation (log-transformed length to width ratio) increases with patch size, with a weaker relationship in highly inundated sites (14, 28). **(b)** Perimeter to area scaling shows a slight curvature (linear model is shown in blue; quadratic model in red) indicating that patch perimeter increases faster than expected for a fractal relationship. **(c)** *r* spectrums show no support for periodic behavior, which is indicated by the absence of any strong peaks.

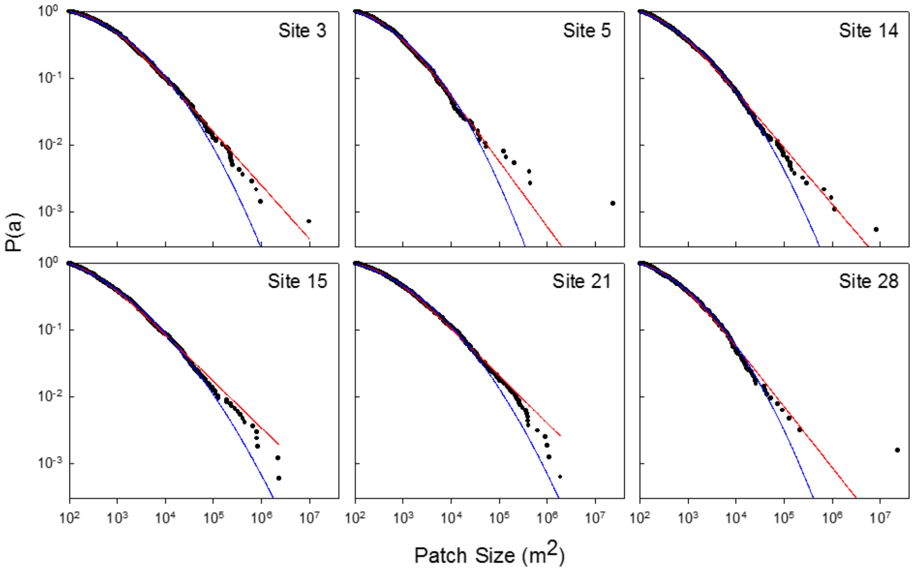

Figure 6. Patch size distributions. Across sites, patch sizes show strong support for the generalized Pareto distribution (shown in red). Sites with high levels of ridge density (e.g. sites 5 and 28) have maximum patch sizes much greater than expected from the GP distribution. Conversely, sites in the deeply inundated southern section of WCA-3A (e.g. sites 15 and 21) show a slight degree of rounding off in the tail end of the distribution. The rounding at the tail end is consistent with the lognormal distribution (shown in blue), although the deviation is not significant enough to rule out the GP for these sites.